Fabrication of tunable plasmonic substrates using a table-top gold coater and a hot plate, their optical characterization, and surface enhanced Raman activity

A. Arora and A. Krishnan,

Citation: Journal of Applied Physics **118**, 154901 (2015); doi: 10.1063/1.4933283
View online: http://dx.doi.org/10.1063/1.4933283
View Table of Contents: http://aip.scitation.org/toc/jap/118/15
Published by the American Institute of Physics

Fabrication of tunable plasmonic substrates using a table-top gold coater and a hot plate, their optical characterization, and surface enhanced Raman activity

A. Arora[1,2] and A. Krishnan[1,2,a)]
[1]*Centre for NEMS and Nano Photonics, Department of Electrical Engineering, Indian Institute of Technology Madras, Chennai 600036, India*
[2]*Experimental Optics Laboratory, Department of Electrical Engineering, Indian Institute of Technology Madras, Chennai 600036, India*

(Received 5 August 2015; accepted 4 October 2015; published online 19 October 2015)

We present a simple scalable technique for repeatable fabrication of large area (cm^2) electromagnetic hot spots using tunable Localized Surface Plasmon Resonance (LSPR) substrates and their k-space microscopic imaging characterization. The substrates were fabricated simply using a low vacuum air plasma scanning electron microscope gold coater and annealing using a hot plate. The measured permittivity profile and optical transmission characteristics of such substrates showed large changes before and after annealing, with clear changes in the occurrence and position of the LSPR in the visible spectrum. Furthermore, the LSPR wavelength of these substrates was tuned from 537 nm to 630 nm using cyclic deposition and annealing. It was observed that every anneal step could be used to blue shift the resonance, while a deposition step could be used to red shift the resonance, thus giving rise to a wide tunability. We also present the k-space images of the substrates using narrowband fluorescence leakage radiation microscopy and broadband polarization microscopy. The enhanced scattering in these substrates was clearly imaged in the k-space, and the color content in the broadband k-space images correlates well with the spectral characteristics of these substrates that can be used in commercial quality testing without a spectrometer. The optical characteristics of the substrates were attributed to the morphology evolution verified using scanning probe microscopy. A single particle model based simulation was used to evaluate the optical response. The substrates were then tested for surface enhanced Raman spectroscopy (SERS) activity using control experiments involving Rhodamine 6G dye in PMMA matrix of different concentrations with analyte volumes of approximately 200 pl and analytical enhancements of $>3 \times 10^4$ (net enhancement $>1.8 \times 10^7$) were obtained. The limit of detection was $\approx 10^{-8}$ M in low volume ($\approx$200 pl) analyte, reaching the regime of few molecule detection. To establish the relevance of the substrates for bio-sensing, surface functionalization using thioglycolic acid was measured using SERS. [http://dx.doi.org/10.1063/1.4933283]

I. INTRODUCTION

Surface Enhanced Raman Spectroscopy (SERS) utilizes high electric field intensity in the vicinity of analyte molecules to enhance the Raman scattering and to obtain the spectral signature of analyte molecules.[1] Recent advances in SERS have enabled low concentration analyte sensing for a variety of applications including biomolecule detection, forensic analysis, and textiles.[2] One of the methods to achieve high local electric field intensity in the vicinity of analytes is by using electromagnetic excitation of noble metal nanostructures resulting in Localized Surface Plasmon Resonances (LSPR). In the recent past, several approaches to design substrates with noble metal nanostructures have been elucidated.[3,4] Common methods in academic research involve noble metal nanostructures of well defined geometries patterned using nanoscale lithography techniques like electron beam lithography,[5] focused ion beam milling,[6] etc. Other approaches involve chemical synthesis and assembly of noble metal nanoparticles on substrates.[7] However, not all of these methods are suitable for a large area (cm^2), use and throw affordable SERS substrates as they either involve the use of sophisticated nanofabrication equipment, high vacuum processes, and/or wet chemical processing. In order to obtain maximum Raman enhancement, relative position of the LSPR wavelength with respect to the excitation and detected Raman peak position of interest has been shown to be critical;[8–10] however, in the above methods, tuning the LSPR wavelength is not very easy, especially, if the total patterned areas are in the order of square centimeters. Commercial substrates mostly make use of chemically or mechanically roughened silicon coated with noble metal or chemically synthesized noble metal nanoparticles over small areas on substrates.[11] Therefore, in order to reduce the complexity and the fabrication cost, there has been increased interest in the fabrication of SERS substrates using simple, unconventional techniques like ink-jet and screen printing of metal nanoparticles,[12,13] metal island films (MIFs),[14,15] and combination of soft-lithography and Nanosphere Lithography

a)Electronic mail: ananthk@iitm.ac.in

(NSL)[16] etc. MIFs exhibit interesting optical properties such as LSPR[17] and are suitable for SERS substrates. Many of the reported works on MIFs utilize high vacuum deposition systems and inert ambience furnaces/oven.[14,15,18–20] Recently, MIFs have been revisited with different approaches like ablation,[21] laser annealing,[22] and electrochemical methods[23] for fabrication of SERS substrates. In order for widespread use of SERS to become a commercial level testing platform, significant process reduction, cost-cutting, and a simple quality check are key issues to be resolved.

In this work, a simple technique for the fabrication of Gold Island Films (Au-IFs) based LSPR substrates without using any nanofabrication equipment or high vacuum process is presented. Au-IFs substrates were fabricated using cyclic thin gold film deposited using a scanning electron microscope (SEM) coater and hot plate annealing of these gold films, on 18 mm × 18 mm microscope cover slips. The optical properties of such substrates were measured systematically, and the LSPR wavelength of the substrates could be tuned from 537 nm to 630 nm. It was observed that in every cycle, a deposition step resulted in a red shift of the LSPR wavelength, while an annealing step resulted in a blue shift of the same, using which the resonance could be tuned to a required LSPR wavelength in the visible spectrum. The Mie scattering properties of such films were imaged using broadband polarization microscopy (PM) in the k-space and verified using fluorescently coupled leakage radiation microscopy. The images clearly showed enhanced scattering by the annealed films, indicating the depercolation of these films on annealing. In the broadband images, the color content in the individual R, G, and B planes could be used to estimate the LSPR position to determine the suitability for SERS applications. Such substrates show promise for large scale manufacturing and quality checks could be performed non-destructively without a spectrometer using a fast k-space optical microscope imaging. However, these substrates could be made easily in an academic laboratory without any significant material processing.

II. GOLD ISLAND FILM BASED LSPR SUBSTRATES

A. Fabrication

Au-IFs were fabricated on glass substrates using SEM gold coater and a hot-plate for post-deposition annealing in open atmosphere. Microscopic glass cover-slips (BK7 18 mm × 18 mm) of thickness 180 μm were used as substrates. Prior to deposition, the substrates were cleaned with Acetone/IPA/DI water, dried in nitrogen followed by a dehydration bake at 120 °C for 10 min. The SEM Gold coater was characterized for the deposition rate and consistency of the film thickness for different deposition times using a Spectroscopic Ellipsometer (SE). The ellipsometric data (Ψ and Δ) at different incidence angles (45°, 55°, 65,° and 75°) and transmittance measurement at normal incidence of the films were recorded and analyzed using ellipsometric data analysis software CompleteEASE^{TM} version 4.63.[24] The optical properties of bare glass substrates (prior to Au deposition) and deposited Au films were measured using Cauchy and B-spline models, respectively,[25,26] and the film thicknesses were extracted. The deposition rate of SEM Gold coater was calculated to be ≈0.6 nm/s and was linear in the range of deposition times starting from 6 s, which was used in the experiments. The measured thickness was found to be consistent with the maximum substrate to substrate variation of ≈4% and point to point variation on a given substrate being significantly small.

After characterizing the deposition process using the SEM Gold coater, substrates with different thicknesses were fabricated and their transmission characteristics were measured from 400 nm to 1200 nm. The transmittance of 6 s and 12 s deposited films is shown in Fig. 1(a). Substrates with ≤6 s deposition time showed a distinct dip in transmission, while substrates with ≥12 s deposition time showed the characteristic transmission spectrum of continuous gold thin films. The properties of metal thin films depend on their morphology, which in turn depend on the method of deposition, deposition parameters, metal being deposited, and the substrate used. Thin film growth starts with the statistical formation of nucleation centers, followed by Volmer-Weber growth[17] that results in island formation. These islands continue to grow until they touch each other and coalesce into a semi-continuous film. After a threshold, called percolation thickness, the properties change abruptly and further increase in thickness often leads to poly-crystalline continuous films.[17,27] For the formation of island thin films, the deposition should be stopped just before the percolation thickness. Therefore, from Fig. 1(a), it was inferred that 6 s deposited film represented Au-IF and 12 s deposited film represented percolated film, and hence the percolation thickness in this Gold film-glass substrate system was measured to be ≈7 nm (corresponding to 12 s film).

The LSPR wavelength of these substrates could not be tuned over a large wavelength range, since in just 12 s of deposition, the films percolate and hence do not show the signature of LSPR. In order to overcome this problem of tunability, these films were subjected to a thermal stress by post-deposition annealing at 250 °C for 120 min on a hot-plate in the open atmosphere. The annealing resulted in a visible color change of the films from blue (or greenish-blue) to pink (or purple-red) for 6 s (or 12 s) deposited films as shown in the insets of Figs. 1(a) and 1(b), indicating some change in surface morphology. Stress (intrinsic and/or thermal) makes the morphological structure of almost all thin

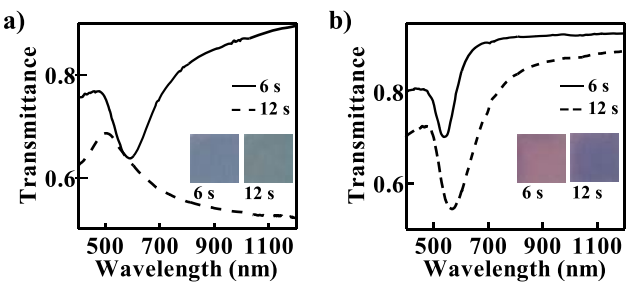

FIG. 1. Transmittance of 6 s and 12 s deposited Au films (a) before and (b) after annealing. Optical images of the substrates are shown in the insets.

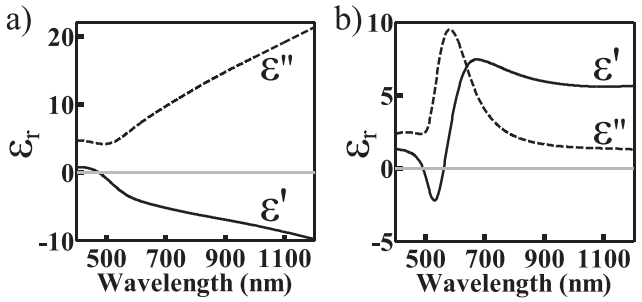

FIG. 2. Extracted permittivity (a) before and (b) after annealing of 12 s deposited film.

films, a non-equilibrium, thermodynamically unstable state, which tends to rearrange the metal atoms on the substrate over very small regions to a minimum energy configuration. The thermal stress arises due to mismatch in thermal coefficients of the deposited metal and the substrate.[28] Post deposition annealing can be considered as a diffusion limited island migration process, where increase in island size and decrease in island density result in restructuring of the surface.[29] Due to the thermal energy, some of the islands execute a random walk (surface diffusion at a given temperature). Upon collision with other islands, they coalesce immediately resulting in an increased island size. The growth process continues until all the mobile islands have been captured by the immobile ones, or due to an increase in the size, they themselves have become immobile. The final morphology of the island thin film, for a given metal-substrate system, depends on annealing temperature, annealing time, and initial film thickness. For the 6 s deposited film, surface modification due to the annealing resulted in a blue shift of LSPR wavelength from 600 nm to 535 nm and flattening of transmission spectrum above 700 nm as shown in Fig. 1(b).

Annealing can also result in island formation in just-percolated films due to thermal dewetting of the substrate if sufficient stress is developed at film-substrate interface.[30] For the 12 s deposited film, which exhibited the property of just-percolated film, after annealing, showed a distinct dip in transmission at ≈570 nm, which was absent prior to annealing as shown in Fig. 1(b). The just-percolated films are semi-continuous with some surface voids, which on annealing depercolates to form discrete islands. However, beyond a critical thickness, discrete island formation does not take place for the given annealing parameters. In our experiments, annealing of 24 s film did not result in a dip in transmittance and therefore was concluded to be more than the critical thickness.

As seen from Figs. 1(a) and 1(b), the 12 s deposited film exhibited a large change in the transmittance before and after annealing. These films were characterized using SE for extracting the change in real (ϵ') and imaginary (ϵ'') parts of relative permittivity (ϵ_r) of the film due to annealing, as shown in Fig. 2. Prior to annealing, the film showed a Drude behavior with a wavelength of 480 nm corresponding to $\epsilon' = 0$ (or plasma frequency) as shown in Fig. 2(a). However, after annealing, the plots of ϵ' and ϵ'' changed to those shown in Fig. 2(b). It can be observed that the ϵ' exhibits a steep zero crossing at 570 nm and, at exactly the same position, ϵ'' peaks to ≈9, which is a signature of electromagnetic resonance. From Figs. 1(b) and 2(b), it is clear that $\lambda_{LSPR} = 570$ nm for this film.

B. k-space imaging characterization and scanning probe microscope verification

In order to develop an imaging based characterization for rapid testing of these substrates, the plasmonic properties of 12 s deposited films were further analyzed using broadband polarization microscope (PM) (schematic of the setup is shown in Fig. 3(a)). A transmission mode inverted optical microscope equipped with 100× oil immersion objective (NA = 1.4) for Fourier Plane (FP) broadband PM was used for scatterometric analysis. In the FP, the intensity distribution as a function of momenta k is imaged and these images provide valuable information regarding the intensity of light scattered at different angles and subsequently transmitted through the substrate in this setup. In bare glass, the maximum scattering was observed at momenta corresponding to the numerical aperture of the collection objective lens as shown in Fig. 3(c). The central bright spot is due to the direct transmission because of the limited extinction efficiency of the cross-axis polarizer-analyzer. The films before and after annealing were imaged under the optical microscope with cross axis polarizer-analyzer configuration, and the FP images before and after annealing were obtained under identical microscopy conditions as shown in Figs. 3(d) and 3(e), respectively. In PM, the light can be collected only if there is scattering (or polarization rotation) by the substrates. Due to the semi-continuous nature, the film prior to annealing showed minimal scattering (Fig. 3(d)), while the scattering was enhanced for the film after annealing, possibly due to the formation of islands, evident from yellowish orange disk shaped emission

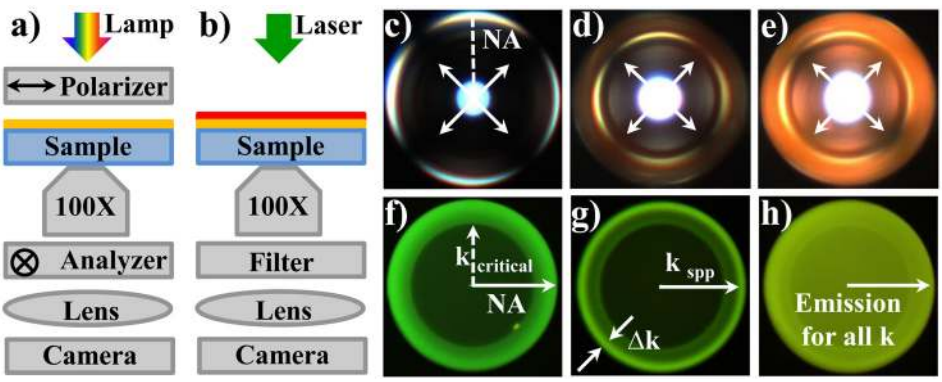

FIG. 3. (a) Broadband PM setup and (b) fluorescence LRM setup. Broadband PM Fourier plane images of (c) bare glass, (d) 12 s deposited film, and (e) 12 s deposited film after annealing. Fluorescence LRM Fourier plane images of Rhodamine doped 130 nm thick PMMA on top of (f) bare glass, (g) 12 s deposited film, and (h) after annealing of 12 s deposited film.

(Fig. 3(e)). An additional feature in the form of a sharp yellow ring was observed in Figures 3(d) and 3(e), while this ring feature was not prominent in the image for the bare glass unless the exposure time was increased, wherein the outermost ring in Fig. 3(c) was saturating the camera (image not shown here for conciseness). On a casual look, these sharp yellow rings in Figures 3(d) and 3(e) appear to be the signature of propagating Surface Plasmons (SPs), leaking through the substrate at specific angles forming a cone shaped emission, a cross section of which is imaged in the FP as reported in a prior work.[31] However, the yellow ring's radius in the FP that is indicative of its momentum (and hence the effective index at the sample air interface) was lower than the reported values of the effective index in the prior works.[31] If indeed this was indicative of the propagating SP excitation at the metal air interface, then loading the substrate with a thin layer of a dielectric like PMMA with index of 1.454 of a thickness 130 nm should significantly increase the effective index of the propagating SP and the radius of the ring should increase considerably in response to this change in effective index. However, on loading the 12 s deposited substrate or the annealed substrate, with a PMMA layer, the radius of the ring did not get altered. Using these two key observations, it was concluded that this feature in these particular experiments occurred due to the total internal reflections occurring in the collection optics of the microscope. In order to confirm this conclusively, high exposure time FP images of the bare microscope setup without any substrate were obtained (not shown here) and the same ring shaped feature was observed at the exact same radius of same color, thus confirming the other related observations, that no propagating SPs were imaged in Figures 3(d) and 3(e).

From Figures 3(a), 3(c), 3(d), and 3(e), the enhanced scattering of the incident light can be clearly seen when the 12 s deposited sample was annealed. The images also indicate the possibility of a morphological change of the metal film when subjected to an annealing step. This was consistent with the spectrometric observations detailed in Section II A of this paper. Such an imaging based characterization of large area (cm^2) substrates could be achieved in a manufacturing environment by placement of polarizing optics and a convex lens in front of the imaging camera, in standard commercial Fast Inline Lens/Micro Lens Testers routinely used in testing mobile phone camera lens wafers in the industry.[32]

The films were also characterized using fluorescence leakage radiation microscope (LRM),[33,34] wherein 1 mM Rhodamine 6G (Rh6G) doped PMMA of 130 nm thickness was used to couple the incoming light to SP at PMMA-Au interface and the radiative decay of SP to light through the substrate due to phase matching conditions was used to study the momentum (k) information from Fourier plane images (schematic of the setup is shown in Fig. 3(b)). For bare glass, the emission was limited by numerical aperture of the collection lens (NA) as the outer radius and critical angle at Air-PMMA-glass interface as the inner radius (shown in Fig. 3(f)). The detailed mechanism for this emission in bare glass coated with a dye doped dielectric has been reported in a recent work.[35] In the case of the film prior to annealing, due to its semi-continuous nature, a weak thin ring shaped emission was observed as shown in Fig. 3(g), due to radiative decay of the propagating SP. The radius of the ring represents the momentum of SP, which in turn indicates the effective index of the SP mode excited on the interface of Au and dielectric superstrate (PMMA). The thickness of the ring in k-space (Δk in Fig. 3(g)), which is the difference between the outer and inner radii of the ring shaped emission, is inversely proportional to the propagation length of SP and therefore indicates that thicker the ring, the lesser is the propagation length of SP. The LRM image of the film after annealing showed emission for all values of momenta (shown in Fig. 3(h)), with complete circular disk shaped emission. It can be viewed as a ring with a very large thickness (thickness now becomes difference between the outer radius and inner radius of the emission), indicating very small propagation length, showing the localized nature of SP, i.e., the excitation of LSPR. Overall, the measured scattering from the annealed sample was 7 times higher than the same sample prior to annealing, which is obtained by the ratio of the net intensity of the images obtained using identical imaging conditions. The image shown in Fig. 3(h) clearly shows the enhanced scattering due to the LSPR excited in these substrates. In the absence of metal nanostructures, however, the FP image obtained will not show scattering related features at $k < k_{critical}$, meaning that no significant scattering occurs to transmit the light through the substrates at angles lower than the critical angle of the substrate/PMMA/air interface.

The surface morphology of the substrates was obtained using Scanning Probe Microscope (SPM) in tapping mode and the formation of islands due to the annealing was confirmed. SPM images of bare glass, the 12 s deposited film, and the same film after annealing are shown in Figs. 4(a)–4(c), respectively. The substrate after annealing showed the formation of islands mostly circular in cross section with a mean size of ≈50 nm and a standard deviation of ≈15 nm.

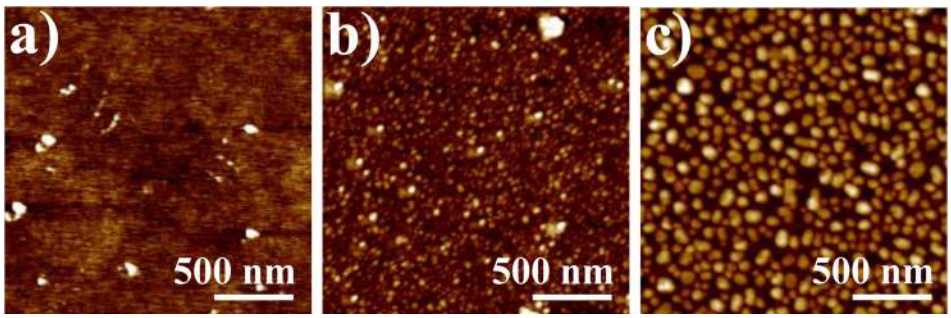

FIG. 4. SPM images of (a) bare glass, (b) 12 s deposited film, (c) 12 s deposited film after annealing.

C. Tuning the resonance wavelength of Au-IFs

The LSPR wavelength (λ_{LSPR}) of Au-IFs depends on the surface morphology and therefore can be tuned by modifying the size/shape of the islands of Au-IFs (we show later in this work why tunability is important for maximizing the SERS activity). This can be achieved by varying the annealing temperature and effective thickness. Annealing time for the substrates was decided based on the visible color change of the substrates, and the parameters used for tuning were annealing temperature and effective thickness. Out of these two parameters, one was fixed in a set of experiment to study the effect of other. The modifications in the spectra are qualitatively explained through a set of suggested mechanisms. These suggested mechanisms were supported by a simple single nanoparticle simulation models using Discrete Dipole Approximation (DDA) method (DDSCAT 7.3).[36] Fig. 5 shows the different methods used for tuning the resonance experimentally (upper row) and their simulation plots based on a suggested model that accounts for annealing and deposition as a modification of particle shape itself (lower row).

For the first set of experiments, to study the effect of annealing, 6 s sputtered Au-IF substrates were annealed at different temperatures for 15 min. A blue shift and narrowing of the spectral dip was observed with increase in annealing temperature. The blue shift can be attributed to the increase in sphericity of the islands on the glass substrate. Au is non-wetting for glass and thus follows Volmer-Weber growth. With the increase in thermal energy, islands would try to reduce the contact area and thus increase the sphericity. This increase in sphericity results in a blue shift and narrowing of resonance dip. This was validated from the simulation of particles with varying ellipticity while maintaining a constant volume, which showed the same trend. In experiments, the narrowing of the dip was also due to the decrease in coupling between the islands because of decreased island density after the annealing. Fig. 5 (column 1) shows the transmittance of Au-IFs annealed at different temperature and a representative model to explain the shift.

For the second set of experiments, to study the effect of varying thickness, substrates with thickness 2 nm to 14 nm (4 s to 24 s coating time) were annealed at 250 °C till the visible color change was observed (≈120 min). Higher temperature was selected to provide sufficient thermal energy to depercolate the films with higher thickness. Red-shift and broadening of resonance dip was observed for substrates with increasing thickness. With the increase in effective thickness, the island size would increase, thus shifting the resonance to a longer wavelength. However, the tunability was limited and resonance beyond 580 nm (for 11 nm film) could not be achieved. This was validated with the simulation of spherical particles of increasing sizes and displayed a similar trend. Films with thickness >11 nm did not show a well defined dip in transmittance, as annealing using the given parameters was not sufficient to depercolate the film and therefore were not considered. Fig. 5 (column 2) shows the transmittance of annealed Au-IFs of varying thicknesses and a representative single particle model to explain the trend. It should be noted that there is quite a difference between the experimental data and simulated data. This is because, in the experiments, there exists a statistical distribution of the size of the islands that resonate at slightly different wavelengths, thus changing the actual position of the resonance and the spectral width compared to a clean single particle model that uses the mean size of these particles only.

Based on the above analysis, the effect on λ_{LSPR} can be summarized as a (i) blue shift on annealing and (ii) red shift on increasing effective thickness. However, it was also inferred that merely increasing the thickness could not result in wide range tunability. Therefore, a scheme of repeated cycles of deposition and annealing was performed to tune the resonance beyond 600 nm. For this, 6 s sputtered substrate (referred as substrate-**a**) was subjected to annealing at 100 °C for 15 min (substrate-**b**), followed by sputtering for 6 s (substrate-**c**), followed by annealing at 100 °C for 15 min (substrate-**d**), and followed by sputtering for 6 s (substrate-**e**). A larger shift was observed using this method as compared to

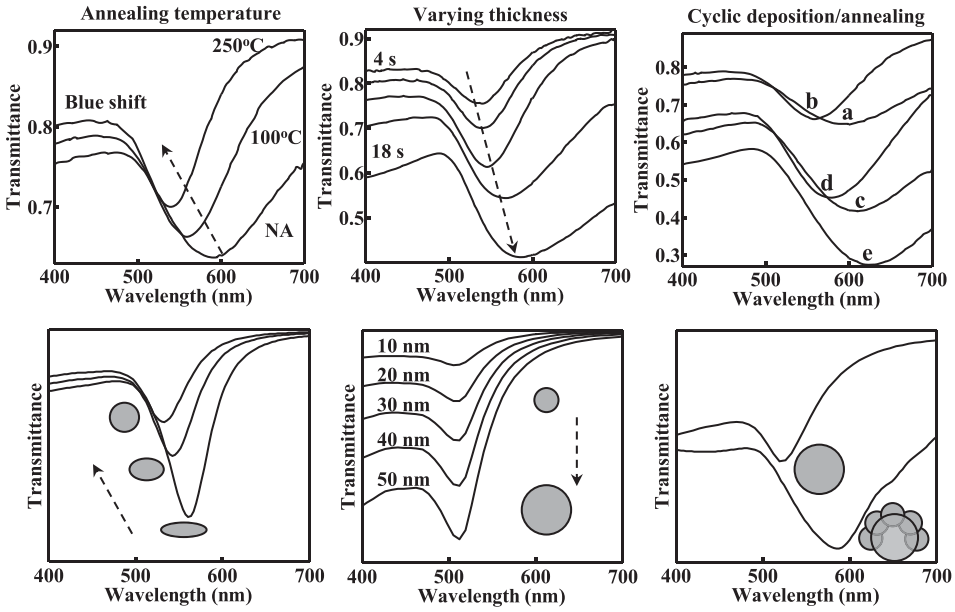

FIG. 5. Different methods used for tuning the resonance wavelength: experiment (upper row) and suggested mechanisms validated using a simulation model (lower row).

the single step deposition and annealing for the same effective thickness. This may be explained as a change in the shape of the islands itself. The first annealing would give rise to spherical islands, and when this substrate is coated with gold, larger islands on the substrate will be surrounded by smaller ones that can result in a red shift. Therefore, the scenario was modeled as a large spherical particle (formed due to annealing), coated by smaller spheres (due to sputtering). The latter showed a red shift and broadening of dip compared to former, which was in concurrence with the experimental results. Fig. 5 (column 3) shows the transmittance of substrates-**a** to **e** and a representative model to explain the shift. Tunability up to 630 nm was obtained by this method. This method can be used to tune λ_{LSPR} over a wide range by varying the parameters of the cycle.

D. SERS activity and enhancement

Raman spectra of the substrates were recorded in reflection mode using a laser excitation of 633 nm delivering 15 mW power focused on the substrates using 100× objective (spot size ≈10μm) with a 10 s integration time. The fabricated Au-IF substrates-**a** to **e**, tuned for their λ_{LSPR}, were spin coated with ≈130 nm thick layer of 10^{-4} M Rh6G doped PMMA for SERS experiments. Bare glass was spin coated with 10^{-2} M Rh6G doped PMMA with same spinning parameters for reference spectrum. Fig. 6 shows the SERS spectra for substrates-**a** to e and the normalized intensity at 1501 cm^{-1} (corresponding to 700 nm for $\lambda_{exc} = 632$ nm) versus λ_{LSPR} with PMMA matrix (red shifted with respect to that shown in Fig. 5 due to refractive index of PMMA). The reference Raman spectrum (Rh6G on bare glass) was flat with no signature peak of Rh6G. The Raman spectra of Rh6G on Au-IF substrates showed enhanced Raman scattered intensity many orders higher than that of Rh6G on bare glass. Excitation of LSPR on Au-IFs leads to strongly enhanced local electromagnetic fields. This enhanced electric field when experienced by the analyte molecules enhances the Raman scattering. This forms the basis of SERS and is known as electromagnetic enhancement. The chemical enhancement could be ignored since Rh6G is not known to interact chemically with the Au-Ifs, and the enhancement can be considered only due to electromagnetic enhancement. The enhancement was found to depend on λ_{LSPR} and the Raman scattered intensity was about three times higher for substrate-**c** than other Au-IF substrates (shown in Fig. 6). The maximum enhancement should be observed when fields at both the wavelengths, excitation (λ_{exc}) and Raman shifted wavelength (λ_R), are enhanced. The electromagnetic Enhancement Factor (EF) therefore depends on the relative position of λ_{LSPR} with respect to λ_{exc} and λ_R and can be given as[8]

$$EF \propto \left| \frac{E_{local}(\lambda_{exc})}{E_{\circ}(\lambda_{exc})} \times \frac{E_{local}(\lambda_R)}{E_{\circ}(\lambda_R)} \right|^2. \quad (1)$$

The maximum enhancement was observed for substrate-**c** whose λ_{LSPR} was closest to the spectral mid-point of λ_{exc} and λ_R. This was consistent with the previously reported relation for λ_{LSPR} for maximum enhancement.[8–10] The magnitude of EF of these substrates was calculated through two different approaches following the definition given in Ref. 37. The first and the most used definition, referred to as substrate enhancement factor (SEF), which considers the enhancement only due to molecules adsorbed on surface for SERS, is given as

$$SEF = \frac{I_{SERS}/N_{surf}}{I_{ref}/N_{vol}}, \quad (2)$$

where I_{SERS} and I_{ref} are the peak intensity of SERS and reference spectrum, respectively; N_{surf} and N_{vol} are the number of analyte molecule (here Rh6G) on surface of SERS substrate and in excitation volume, respectively. For substrate-**c**, maximum $I_{SERS} = 9.2 \times 10^3$ counts. For bare glass, with the same parameters and thickness of analyte layer, no signature of Rh6G was obtained even with 10^{-2}M solution; therefore, maximum intensity at the same spectral position, $I_{ref} = 30$, which was the noise floor, was used.

The excitation volume was ≈2×10^{-17} m^3 (200 pl), therefore for 10^{-2}M solution, the number of molecules in the given volume on reference substrate was 12×10^7. For the calculation of N_{surf}, it was assumed that the surface area on the substrate is equal to the area illuminated by the laser and the enhancement is only for a single layer of molecules. The area fraction of Rh6G in PMMA matrix was approximately taken equal to the volume fraction. The volume fraction of Rh6G in solution of 10^{-4} M concentration was calculated to

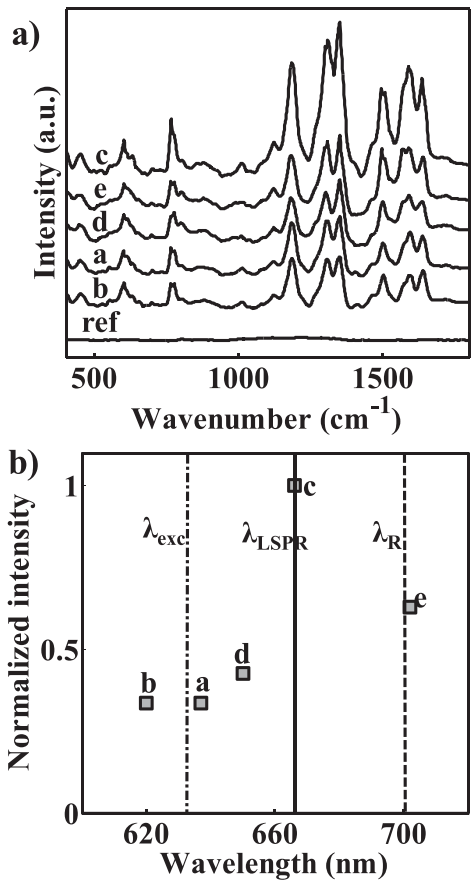

FIG. 6. (a) SERS spectra of Rh6G on substrates labeled **a** to **e** and (b) Raman scattered intensity, normalized with respect to the substrate-**c**, of the peak at 1501 cm^{-1} versus λ_{LSPR} of these substrates.

be 3.8×10^5, and this gives the total surface area of Rh6G as $3.8 \times 10^{-15}\,m^2$. Area of one Rh6G molecule was taken to be $2 \times 10^{-18}\,m^2$ as reported in prior works,[38] and this gives $N_{surf} = 2000$. Using these values in Eq. (2), $EF = 1.8 \times 10^7$. Since the reference substrate could not give signature spectrum of Rh6G even for 10^{-2} M and higher integration time, it can be said that $EF > 1.8 \times 10^7$. Calculation of SERS EF using this method involved many assumptions and not suitable for an end user. A more intuitive definition, involving only the analytical parameters like concentration of analyte and peak intensity, called analytical enhancement factor (AEF) was used. According to the definition given in Ref. 37

$$AEF = \frac{I_{SERS}/c_{SERS}}{I_{ref}/c_{ref}}, \tag{3}$$

where c_{SERS} and c_{ref} are the concentrations of the solutions used for SERS and reference spectrum. This gives $AEF = 3 \times 10^4$.

Since a correlation was observed between SERS EF and λ_{LSPR}, an indirect method to characterize these substrates for their EF is proposed using the broadband PM as discussed before in Fig. 3(a). The significant color changes occurring in the Fourier plane images from the broadband polarization microscopy of the substrates a through e exhibited a strong correlation with the measured shifts in λ_{LSPR} of these substrates. A quadrant of these images excluding the direct transmission for the substrates a and e were analyzed for their RGB components. The images with their mean values of Red (R) and Blue (B) components and their standard deviation are shown in Fig. 7. The mean value of R reflects the position of dip and the standard deviation represents the width of the resonance dip. This method of characterization is a novel technique and can be used as a simple method to ascertain the resonance wavelengths from the color content of FP images for a given microscope setup.

For comparison of SERS enhancements of Au-IFs, triangular nanostructures using another popular method, NSL, were fabricated over an area of $\approx 2\,cm^2$. Technique based on pre-assembly of PolyStyrene NanoSpheres (PSNS) at air-water interface followed by transfer to the substrate, as given in Ref. 39, was used for large area, close pack monolayer PSNS colloidal crystal formation. These substrates were then coated with 2 nm chromium (for adhesion) and 30 nm gold using electron beam evaporation system. The gold coated

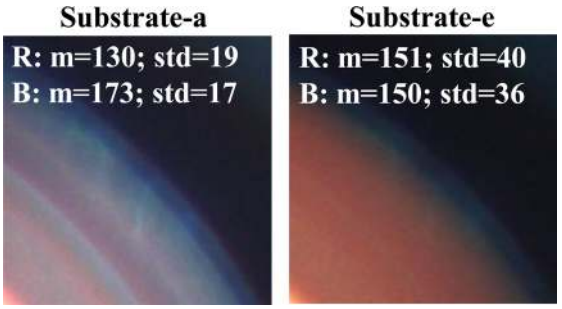

FIG. 7. A quadrant of the Fourier plane PM image of substrates **a** and **e**. The mean and the standard deviation of red and blue components of the RGB image, normalized with respect to its total intensity, are shown.

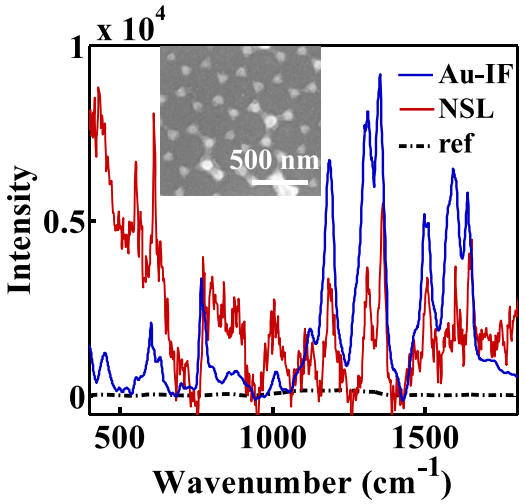

FIG. 8. SERS spectra for NSL and Au-IF substrates. SEM image of fabricated NSL substrate is also shown.

substrates were sonicated in ethanol for 30 s to lift-off the PSNS leaving the 50 nm sides triangular nanostructures in hexagonal voids on the substrates. A few of these substrates were used as such without lift-off for comparison purposes and will be referred to as Au coated PSNS. For SERS measurements, the fabricated substrates were coated with 10^{-4} M Rh6G using the same parameters as that of Au-IF substrates and the obtained SERS spectra are shown in Fig. 8. The AEF of the fabricated NSL substrates was calculated to be 1.7×10^4. The spectrum obtained for NSL substrate was noisy and AEF was approximately half the AEF of Au-IF substrates. This may be due to low density of active sites as the hexagonal close pack has 90% packing efficiency, therefore after lift-off leaving active sites, only over 10% of the total area on the substrate. Furthermore, the AEF of Au-IF substrates was also compared with Au coated PSNS (without lift-off). The AEF of Au coated PSNS was in the same order as Au-IF. Hence, the Au-IF is definitely a simpler method for fabrication of such substrates.

The Au-IF substrates were tested for their limit of detection of analyte. The substrates were spin coated with

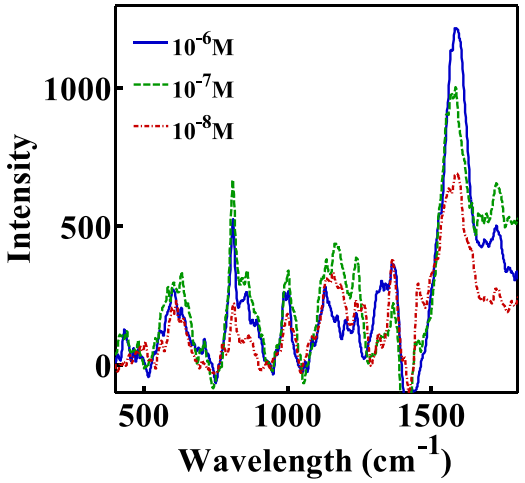

FIG. 9. SERS spectrum of low concentration (10^{-8}M) low volume (200 pl) Rh6G in PMMA matrix.

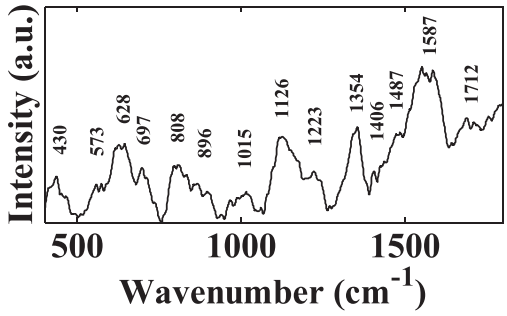

FIG. 10. SERS spectrum of TGA functionalized Au-IF substrate.

different concentrations of Rh6G. The SERS spectrum of concentrations 10^{-5} M and higher showed sharp peaks corresponding to Rh6G. For concentrations 10^{-6} M and lower, the signals from PMMA were of comparable strength, hence peaks related to both Rh6G and PMMA were observed. These substrate were able to detect Rh6G for concentration as low as 10^{-8} M. However, the signal to noise ratio was poor and peaks related to both Rh6G and PMMA were observed (shown in Fig. 9).[40–42] For this concentration, the number of Rh6G molecules in the excitation volume was around 120. As a crude approximation using the method given above, at this concentration, N_{surf} become less than 1, i.e., having a molecule on surface becomes probabilistic. Hence, the only logical conclusion to arrive at is that these SERS substrates are able to detect analyte (Rh6G) to a regime of few molecules.

The Au-IF substrates were finally tested for their potential application in biosensing, by obtaining the Raman fingerprints of a surface functionalization layer, whose Raman vibrational spectra have been reported in prior works.[43–45] SERS substrates for biological sensing applications are usually functionalized to increase selectivity. Surface functionalization techniques also bring the analyte closer to the noble-metal structure and therefore increasing enhancement. Commonly used chemicals for surface functionalization are alkanethiolates, and these molecules anchor to the noble-metal surface by a thiolate group and form self-assembled monolayer (SAM). The SAM can separate the analyte of interest from interfering analytes and bring it closer to the nanostructured surface. For the experiment, Thioglycolic acid (TGA), a two carbon alkanethiolate, was used to functionalize the substrate. The fabricated Au-IF substrates were incubated in 1 mM TGA (1.4 μl TGA in 20 ml ethanol) over night at room temperature and gently washed in ethanol. The substrates were then left to dry in open atmosphere and used for Raman spectrum. The SERS spectrum of SAM layer of TGA is shown in Fig. 10. The spectrum showed clear signatures of TGA for all possible orientations on the substrate reported in the past.[43–45]

III. CONCLUSION

In this work, a simple technique for the fabrication of Au-IF SERS substrates without using any high vacuum process and nanofabrication equipment was presented. These substrates were characterized for their optical properties. A simple scheme of repeated deposition using a SEM coater and annealing using a hot plate was presented for tuning the resonance wavelength (λ_{LSPR}) of these substrates over a wide range. A method to characterize these substrates using Fourier plane PM images was discussed, which can be developed as a potential quality check method for these substrates on large scale. SERS analytical EF $>3 \times 10^4$ (and net enhancement factor $>1.8 \times 10^7$) was achieved for these substrates. As a general and more intuitive parameter, AEF of these substrates was calculated and was found comparable to that of Au coated PSNS and NSL substrates. These substrates were able to detect low concentration low volume analyte reaching the regime of few molecules detection. These substrates were functionalized with TGA and shown to have potential for bio-sensing applications. Therefore, considering the complexity involved in fabrication and the performance of the substrates, Au-IF substrates show a great potential as large area affordable SERS substrate.

ACKNOWLEDGMENTS

The authors would like to thank Centre for NEMS and Nano Photonics (CNNP) for the use of fabrication facilities. The authors would like to thank Professor M. S. Ramachandra Rao for allowing us to use the Scanning Probe Microscopy facility at the Nano Functional Materials Technology Center (NFMTC). A. Krishnan thanks Dr. Kyoyeon Park for many fruitful discussions.

[1]P. L. Stiles, J. A. Dieringer, N. C. Shah, and R. P. Van Duyne, "Surface-enhanced Raman spectroscopy," Annu. Rev. Anal. Chem. **1**, 601–626 (2008).
[2]L. A. Nafie, "Recent advances in linear and nonlinear Raman spectroscopy. Part VIII," J. Raman Spectrosc. **45**, 1326–1346 (2014).
[3]M. Fan, G. F. Andrade, and A. G. Brolo, "A review on the fabrication of substrates for surface enhanced Raman spectroscopy and their applications in analytical chemistry," Anal. Chim. Acta **693**, 7–25 (2011).
[4]S.-C. Luo, K. Sivashanmugan, J.-D. Liao, C.-K. Yao, and H.-C. Peng, "Nanofabricated SERS-active substrates for single-molecule to virus detection in vitro: A review," Biosens. Bioelectron. **61**, 232–240 (2014).
[5]N. Félidj, J. Aubard, G. Lévi, J. Krenn, M. Salerno, G. Schider, B. Lamprecht, A. Leitner, and F. Aussenegg, "Controlling the optical response of regular arrays of gold particles for surface-enhanced Raman scattering," Phys. Rev. B **65**, 075419 (2002).
[6]Y.-Y. Lin, J.-D. Liao, Y.-H. Ju, C.-W. Chang, and A.-L. Shiau, "Focused ion beam-fabricated Au micro/nanostructures used as a surface enhanced Raman scattering-active substrate for trace detection of molecules and influenza virus," Nanotechnology **22**, 185308 (2011).
[7]M. Chekini, P. Oulevey, and T. Bürgi, "Large-scale plasmonic-SERS templates by successive growth steps," Curr. Appl. Phys. **15**, 253–260 (2015).
[8]N. Felidj, J. Aubard, G. Levi, J. Krenn, A. Hohenau, G. Schider, A. Leitner, and F. Aussenegg, "Optimized surface-enhanced Raman scattering on gold nanoparticle arrays," Appl. Phys. Lett. **82**, 3095–3097 (2003).
[9]J. D. Driskell, R. J. Lipert, and M. D. Porter, "Labeled gold nanoparticles immobilized at smooth metallic substrates: Systematic investigation of surface plasmon resonance and surface-enhanced Raman scattering," J. Phys. Chem. B **110**, 17444–17451 (2006).
[10]N. G. Greeneltch, M. G. Blaber, G. C. Schatz, and R. P. Van Duyne, "Plasmon-sampled surface-enhanced Raman excitation spectroscopy on silver immobilized nanorod assemblies and optimization for near infrared ($\lambda_{ex} = 1064$ nm) studies," J. Phys. Chem. C **117**, 2554–2558 (2013).
[11]Commercial SERS substrates, see http://oceanoptics.com/, http://www.renishawdiagnostics.com/, http://atoid.com/, http://www.silmeco.com/, http://www.q-sers.com/.
[12]J. F. Betz, W. Y. Wei, Y. Cheng, I. M. White, and G. W. Rubloff, "Simple SERS substrates: Powerful, portable, and full of potential," Phys. Chem. Chem. Phys. **16**, 2224–2239 (2014).

[13]W. Wu, L. Liu, Z. Dai, J. Liu, S. Yang, L. Zhou, X. Xiao, C. Jiang, and V. A. Roy, "Low-cost, disposable, flexible and highly reproducible screen printed SERS substrates for the detection of various chemicals," Sci. Rep. **5**, Article No. 10208, 1–9 (2015).
[14]J. Perumal, K. V. Kong, U. Dinish, R. M. Bakker, and M. Olivo, "Design and fabrication of random silver films as substrate for SERS based nano-stress sensing of proteins," RSC Adv. **4**, 12995–13000 (2014).
[15]S.-U. Fang, C.-L. Hsu, T.-C. Hsu, M.-Y. Juang, and Y.-C. Liu, "Surface roughness-correlated sers effect on Au island-deposited substrate," J. Electroanal. Chem. **741**, 127–133 (2015).
[16]M. Kahraman, P. Daggumati, O. Kurtulus, E. Seker, and S. Wachsmann-Hogiu, "Fabrication and characterization of flexible and tunable plasmonic nanostructures," Sci. Rep. **3**, Article No. 3396, 1–9 (2013).
[17]N. Kaiser, "Review of the fundamentals of thin-film growth," Appl. Opt. **41**, 3053–3060 (2002).
[18]L. Maya, C. Vallet, and Y. Lee, "Sputtered gold films for surface-enhanced Raman scattering," J. Vac. Sci. Technol. A **15**, 238–242 (1997).
[19]R. Van Duyne, J. Hulteen, and D. Treichel, "Atomic force microscopy and surface-enhanced Raman spectroscopy. I. Ag island films and Ag film over polymer nanosphere surfaces supported on glass," J. Chem. Phys. **99**, 2101–2115 (1993).
[20]M. Lončarić, J. Sancho-Parramon, H. Zorc, S. Šegota, P. Dubček, and S. Bernstorff, "Optical and structural characterization of gold island films on glass substrates," Thin Solid Films **591**, 204–209 (2015).
[21]A. Chou, E. Jaatinen, R. Buividas, G. Seniutinas, S. Juodkazis, E. L. Izake, and P. M. Fredericks, "SERS substrate for detection of explosives," Nanoscale **4**, 7419–7424 (2012).
[22]M. D. Ooms, Y. Jeyaram, and D. Sinton, "Disposable plasmonics: Rapid and inexpensive large area patterning of plasmonic structures with CO_2 laser annealing," Langmuir **31**, 5252–5258 (2015).
[23]T. Ignat, M.-A. Husanu, R. Munoz, M. Kusko, M. Danila, and C. M. Teodorescu, "Gold nano-island arrays on silicon as SERS active substrate for organic molecule detection," Thin Solid Films **550**, 354–360 (2014).
[24]CompleteEASE version 4.63 Data Analysis Manual, J. A. Woollam Co., Inc., 2011.
[25]T. Oates, H. Wormeester, and H. Arwin, "Characterization of plasmonic effects in thin films and metamaterials using spectroscopic ellipsometry," Prog. Surf. Sci. **86**, 328–376 (2011).
[26]M. Lončarić, J. Sancho-Parramon, and H. Zorc, "Optical properties of gold island films, a spectroscopic ellipsometry study," Thin Solid Films **519**, 2946–2950 (2011).
[27]M. Ohring, *Materials Science of Thin Films* (Academic Press, 2001).
[28]J. A. Thornton and D. Hoffman, "Stress-related effects in thin films," Thin Solid Films **171**, 5–31 (1989).
[29]J. R. Levine, J. Cohen, and Y. Chung, "Thin film island growth kinetics: A grazing incidence small angle x-ray scattering study of gold on glass," Surf. Sci. **248**, 215–224 (1991).
[30]A. B. Tesler, B. M. Maoz, Y. Feldman, A. Vaskevich, and I. Rubinstein, "Solid-state thermal dewetting of just-percolated gold films evaporated on glass: Development of the morphology and optical properties," J. Phys. Chem. C **117**, 11337–11346 (2013).
[31]A. Giannattasio and W. Barnes, "Direct observation of surface plasmon-polariton dispersion," Opt. Express **13**, 428–434 (2005).
[32]M. Dahl, S. Heinisch, S. Krey, S. Baumer, J. Lurquin, and L. Chen, "Ultra-fast MTF test for high-volume production of CMOS imaging cameras," in SPIE Conference on Optical Manufacturing and Testing (2003), Vol. 5180.
[33]A. Drezet, A. Hohenau, D. Koller, A. Stepanov, H. Ditlbacher, B. Steinberger, F. Aussenegg, A. Leitner, and J. Krenn, "Leakage radiation microscopy of surface plasmon polaritons," Mater. Sci. Eng., B **149**, 220–229 (2008).
[34]S. Frisbie, C. Regan, A. Krishnan, C. Chesnutt, J. Ajimo, A. Bernussi, and L. G. de Peralta, "Characterization of polarization states of surface plasmon polariton modes by Fourier-plane leakage microscopy," Opt. Commun. **283**, 5255–5260 (2010).
[35]C. J. Regan, D. Dominguez, L. Grave de Peralta, and A. A. Bernussi, "Far-field optical superlenses without metal," J. Appl. Phys. **113**, 183105 (2013).
[36]B. T. Draine and P. J. Flatau, "User guide for the discrete dipole approximation code DDSCAT 7.3," preprint arXiv:1305.6497 (2013).
[37]E. Le Ru, E. Blackie, M. Meyer, and P. G. Etchegoin, "Surface enhanced Raman scattering enhancement factors: A comprehensive study," J. Phys. Chem. C **111**, 13794–13803 (2007).
[38]A. Kudelski, "Raman studies of rhodamine 6G and crystal violet submonolayers on electrochemically roughened silver substrates: Do dye molecules adsorb preferentially on highly SERS-active sites?" Chem. Phys. Lett. **414**, 271–275 (2005).
[39]J.-T. Zhang, L. Wang, D. N. Lamont, S. S. Velankar, and S. A. Asher, "Fabrication of large-area two-dimensional colloidal crystals," Angew. Chem., Int. Ed. **51**, 6117–6120 (2012).
[40]M. Baia, L. Baia, and S. Astilean, "Gold nanostructured films deposited on polystyrene colloidal crystal templates for surface-enhanced Raman spectroscopy," Chem. Phys. Lett. **404**, 3–8 (2005).
[41]R. Li, H. Li, S. Pan, K. Liu, S. Hu, L. Pan, Y. Guo, S. Wu, X. Li, and J. Liu, "Surface-enhanced Raman scattering from rhodamine 6G on gold-coated self-organized silicon nanopyramidal array," J. Mater. Res. **28**, 3401–3407 (2013).
[42]H. Willis, V. Zichy, and P. Hendra, "The laser-raman and infra-red spectra of poly (methyl methacrylate)," Polymer **10**, 737–746 (1969).
[43]A. Królikowska, A. Kudelski, A. Michota, and J. Bukowska, "Sers studies on the structure of thioglycolic acid monolayers on silver and gold," Surf. Sci. **532–535**, 227–232 (2003).
[44]J. Castro, M. López-Ramírez, S. Centeno, and J. Otero, "Adsorption of mercaptoacetic acid on a colloidal silver surface as investigated by Raman spectroscopy," Biopolymers **74**, 141–145 (2004).
[45]J.-G. Zhou, Q. L. Williams, and R. Wu, "Thioglycolic acid on the gold 111 surface and Raman vibrational spectra," J. Chem. Phys. **132**, 064702 (2010).